



## Revised Requirements on the Readout of the Luminosity Calorimeter

H. Abramowicz, R. Ingbir, S. Kananov, A. Levy, I. Sadeh

School of Physics and Astronomy, The Raymond and Beverly Sackler Faculty of Exact  
Sciences, Tel Aviv University, Tel Aviv, Israel.

On behalf of the FCAL collaboration \*

September 2008

### Abstract

A study was performed to define the constraints on the electronic readout for the revised design of the proposed luminosity detector of the International Linear Collider. The required dynamical range was studied by simulating the passage of minimum ionizing particles and of electrons at the nominal energy of 250 GeV through the detector. The minimal required digitization constant was determined, and the issue of channel occupancy was addressed.

---

\*List of members can be found at: <http://www-zeuthen.desy.de/ILC/fcal/>

# 1 Introduction

The focus of this study is the luminosity calorimeter (LumiCal) of the International Linear Collider (ILC). The requirement for LumiCal is to enable a measurement of the integrated luminosity with a relative precision of about  $10^{-4}$  [1]. Bhabha scattering is used as the gauge process for the luminosity measurement. This is motivated by the fact that the cross-section of Bhabha scattering is large and dominated by electromagnetic processes, and thus can be calculated with very high precision [2, 3, 4, 5, 6].

Presently, two detectors are considered for the ILC with the pull-and-push scheme. Within the next half a year, letters of intent are expected. The European high energy committee, which has been working on the fifth version of the so-called “Large Detector Concept” (LDC) [7], has recently joined forces with the Japanese and American communities to promote the International Large Detector (ILD) [8] concept.

In the current ILD layout, LumiCal is placed 2.27 m from the interaction point (IP). LumiCal is a tungsten-silicon sandwich calorimeter. In the revised design of LumiCal, the inner radius stands at 80 mm, and the outer radius at 190 mm, resulting in a polar angular coverage of 35 to 84 mrad. The longitudinal part of the detector consists of layers, each composed of 3.5 mm of tungsten, which is equivalent to 1 radiation length thickness. Behind each tungsten layer there is a 0.6 mm ceramic support, a 0.3 mm silicon sensors plane, and a 0.1 mm gap for electronics. LumiCal is comprised of 30 longitudinal layers. The transverse plane is subdivided in the radial and azimuthal directions. The number of radial divisions is 64, and the number of azimuthal divisions is 48. Figure 1 presents the segmentation scheme of a LumiCal sensor plane.

## 1.1 Energy Resolution

LumiCal is designed such that incident high energy electrons and photons deposit practically all of their energy in the detector. Energy degradation is achieved by the creation of electromagnetic (EM) showers, due to the passage of particles in the layers of tungsten. Prevention of leakage through the edges of LumiCal is possible by defining fiducial cuts on the minimal and on the maximal reconstructed polar angle of the particle showering in LumiCal.

Stable energy resolution is the hallmark of well-contained showers. The relative energy resolution,  $\sigma_E/E$ , is usually parametrized as

$$\frac{\sigma_E}{E} = \frac{a_{res}}{\sqrt{E_{beam} \text{ (GeV)}}}, \quad (1)$$

where  $E$  and  $\sigma_E$  are, respectively, the most probable value, and the root-mean-square of the signal distribution for a beam of electrons of energy  $E_{beam}$ . Very often the parameter  $a_{res}$  is quoted as resolution, a convention which will be followed here. The fiducial volume

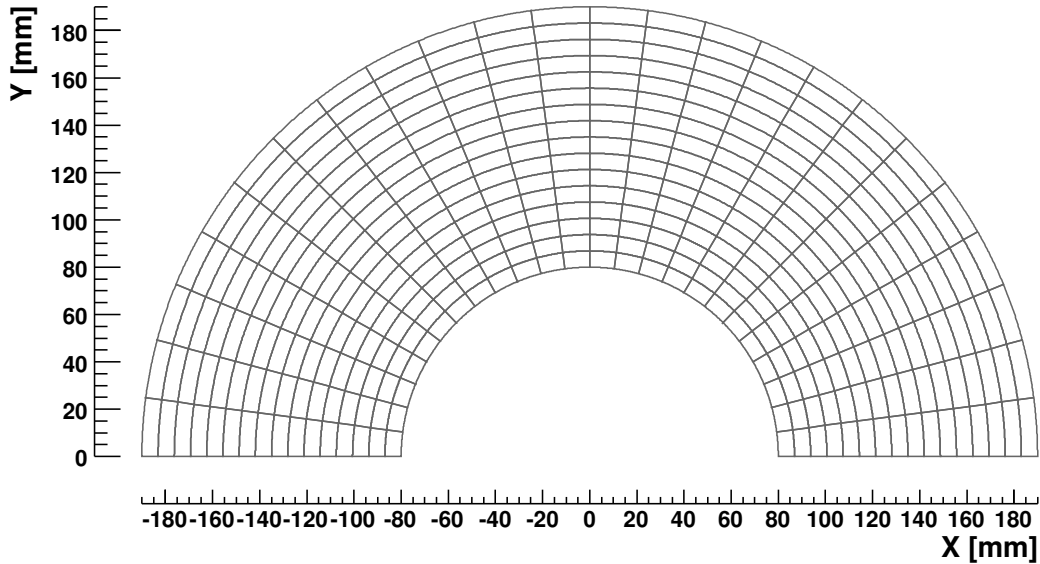


Figure 1: Half plane of LumiCal silicon sensors (every fourth radial segment is drawn).

of LumiCal is defined to be within the polar angular range  $41 < \theta < 69$  mrad. For this fiducial volume  $a_{res} = 21.00 \pm 0.05 \sqrt{(\text{GeV})}$  [9, 10].

## 1.2 Reconstruction of the Polar Angle

The polar angle is reconstructed by averaging over the individual cells hit in the detector, using the cell centers and a weight function,  $\mathcal{W}_i$ , such that

$$\langle \theta \rangle = \frac{\sum_i \theta_i \cdot \mathcal{W}_i}{\sum_i \mathcal{W}_i}. \quad (2)$$

Weights are determined by the so-called logarithmic weighting [11], for which

$$\mathcal{W}_i = \max\left\{ 0, \mathcal{C} + \ln \frac{E_i}{E_{tot}} \right\}, \quad (3)$$

where  $E_i$  is the individual cell energy,  $E_{tot}$  is the total energy in all cells, and  $\mathcal{C}$  is a constant. In this way, an effective cutoff is introduced on individual hits, and only cells which contain a high percentage of the event energy contribute to the reconstruction.

The polar resolution,  $\sigma_\theta$ , and the polar bias,  $\Delta\theta$ , are, respectively, the root-mean-square and the most probable value of the distribution of the difference between the reconstructed and the generated polar angles. The existence of  $\Delta\theta$  is due to the non-linear

transformation between the global coordinate system of the detector, and the coordinate system of LumiCal, in which the shower position is reconstructed. There is an optimal value for  $\mathcal{C}$ , for which  $\sigma_\theta$  is minimal. For this value, the polar resolution and bias of LumiCal are  $\sigma_\theta = (2.18 \pm 0.01) \cdot 10^{-2}$  mrad and  $\Delta\theta = (3.2 \pm 0.1) \cdot 10^{-3}$  mrad, respectively [9, 10].

### 1.3 Error on the Luminosity Measurement

For small angles ( $\leq 10^\circ$ ), Bhabha scattering is dominated by the  $t$ -channel exchange of a photon [12]. One can write the cross-section,  $\sigma_B$ , as

$$\frac{d\sigma_B}{d\theta} = \frac{2\pi\alpha_{em}^2}{s} \frac{\sin\theta}{\sin^4(\theta/2)} \approx \frac{32\pi\alpha_{em}^2}{s} \frac{1}{\theta^3}, \quad (4)$$

where the scattering angle,  $\theta$ , is the angle of the scattered lepton with respect to the beam,  $\alpha_{em}$  is the fine structure constant, and  $s$  is the center-of-mass energy squared.

This means that the total Bhabha cross-section within the angular range  $[\theta_{min}, \theta_{max}]$  is

$$\sigma_B \sim \frac{1}{2} (\theta_{min}^{-2} - \theta_{max}^{-2}) \sim \frac{1}{2} \theta_{min}^{-2}, \quad (5)$$

where the  $\theta_{max}$  dependence can be neglected. To measure the integrated luminosity,  $\mathcal{L}$ , one counts the number of Bhabha events,  $N_B$ , registered in LumiCal, using the respective integrated cross-section,

$$\mathcal{L} = \frac{N_B}{\sigma_B}. \quad (6)$$

The relative error on the luminosity is, therefore, proportional to the relative error on the Bhabha cross-section,

$$\frac{\Delta\mathcal{L}}{\mathcal{L}} \approx 2 \frac{\Delta\theta}{\theta_{min}}. \quad (7)$$

The analytic approximation of Eq. (7) has been shown to hold well in practice [13, 14]. Its implication is that the polar bias,  $\Delta\theta$ , and the minimal polar bound of the fiducial volume,  $\theta_{min}$ , are the two most important parameters that affect the precision of the luminosity measurement. The steep fall of the Bhabha cross-section with the polar angle translates into significant differences in the counting rates of Bhabha events, for small changes in the angular acceptance range.

## 2 Readout Scheme

For a given granularity of LumiCal, it is necessary to define the dynamical range of the electronics required to process the signal from the detector. Once the dynamical range is set, the digitization scheme depends on the ADC precision. The energy resolution depends in turn on the digitization scheme. For the present study, it is assumed that the dynamical range of the electronics has to be such, that it enables to measure signals from minimum ionizing particles (MIP) up to the highest-energy EM showers, which are allowed by kinematics.

In order to determine the lower bound on the signal in LumiCal, the passage of muons through the detector was simulated. Muons do not shower, and are, therefore, MIPs. In the present conceptual approach, muons will be used to inter-calibrate the cells of the detector, and may also be used to check *in-situ* the alignment of the detector [15]. The detection of muons in the forward region also has significance for many searches for physics beyond the Standard Model, such as implied by certain supersymmetry models, or by theories with universal extra dimensions [16].

In order to measure the signals of both MIPs and high energy electrons in LumiCal, the detector would have to operate in two different modes, as discussed below. In the *calibration* (high gain) mode, the electronics will be sensitive to MIP signals. In the *physics* (low gain) mode, the signals of high energy showers will be processed. The signature of a Bhabha event is an  $e^+e^-$  pair, where the leptons are back to back and carry almost all of the initial energy. For the case of a nominal center of mass energy of 500 GeV, the maximal energy to be absorbed in LumiCal is, therefore, 250 GeV, and so 250 GeV electrons were used to find the upper bound on the detector signal. The low limit on the signal will have to be of the order of a single MIP, and will be precisely determined according to the restrictions imposed by the energy resolution.

The response of LumiCal to the passage of particles was simulated using MOKKA, version 06-05-p02 [17]. MOKKA is an application of a general purpose detector simulation package, GEANT4, of which version 9.0.p01 was used [18]. The output of Mokka is in terms of energy lost in the active material, silicon in the case of LumiCal. In order to translate the energy signal into units of charge, the following formula was used:

$$\mathcal{S}_Q[\text{fC}] = \frac{1.6 \cdot 10^{-4}}{3.67} \mathcal{S}_\varepsilon[\text{eV}] \quad (8)$$

where  $\mathcal{S}_\varepsilon$  denotes the signal in units of eV, and  $\mathcal{S}_Q$  the signal in units of fC. The value 3.67 eV is the energy to create an electron-hole pair in silicon. The number  $1.6 \cdot 10^{-4}$  fC is the charge of an electron.

### 3 Dynamical Range of the Signal

The distribution of the energy deposited in a detector cell by 250 GeV muons is presented in Fig. 2. According to this, the most probable value (MPV) of induced charge for a muon traversing 300  $\mu\text{m}$  of silicon is 89 keV, which is equivalent to 3.9 fC.

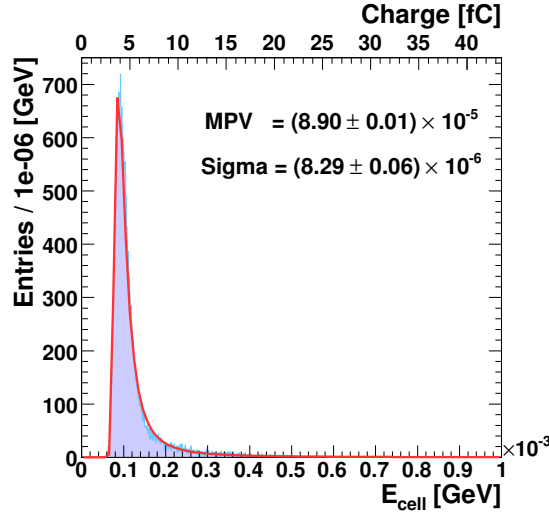


Figure 2: Distribution of the energy deposited in a detector cell,  $E_{cell}$ , by 250 GeV muons. A corresponding scale in units of charge is also shown.

The distribution of collected charge per cell for 250 GeV electron showers is presented in Fig. 3a. The value of the collected charge extends up to 6 pC, which is equivalent to  $\sim 1540$  MIPs. The distribution of the maximal charge collected in a single cell per shower for 250 GeV electrons is shown in Fig. 3b. The distribution extends up to 6 pC.

### 4 Digitization of the Signal

Once a low or high bound on the dynamical range for each mode of operation is set, it is necessary to digitize the signal. For each mode of operation separately

$$\sigma_{\text{ADC}} \equiv q_{\text{min}} = \frac{q_{\text{max}}}{2^{\mathcal{B}_{\text{digi}}}}, \quad (9)$$

where  $\sigma_{\text{ADC}}$  is the ADC channel resolution (bin size),  $q_{\text{min}}$  and  $q_{\text{max}}$  are, respectively, the low and high charge bounds and  $2^{\mathcal{B}_{\text{digi}}}$  is the number of channels for a given number of available ADC bits,  $\mathcal{B}_{\text{digi}}$ . Each cell of deposited charge,  $q_{\text{dep}}$ , is read-out as having a charge,  $q_{\text{digi}}$ , (rounding error) where

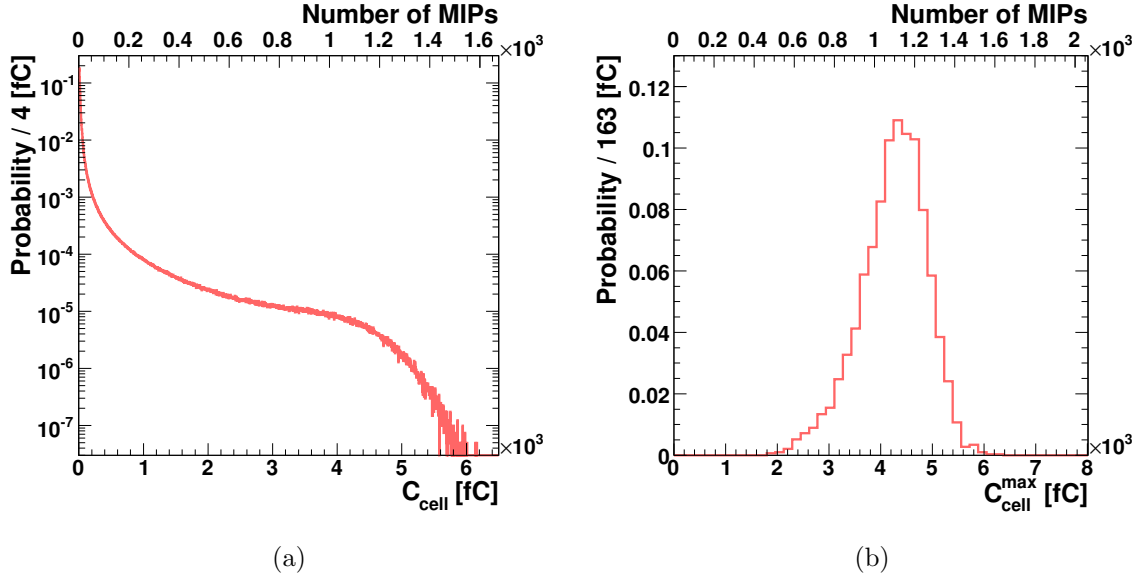


Figure 3: (a) Normalized distribution of the charge deposited in a detector cell,  $C_{cell}$ , by 250 GeV electron showers. (b) Normalized distribution of the maximal charge collected in a single cell per shower,  $C_{cell}^{max}$ , for 250 GeV electron showers. In both figures a corresponding scale in units of MIPs is also shown.

$$q_{digi} = (\mathcal{Q}(q_{dep}, \sigma_{ADC}) + 0.5) \cdot \sigma_{ADC} , \quad (10)$$

and the quotient of the deposited charge with the ADC resolution,  $\mathcal{Q}(q_{dep}, \sigma_{ADC})$ , is defined such that

$$\begin{aligned} \alpha &= \mathcal{Q}(\alpha, \beta) \cdot \beta + \gamma, \\ 0 &\leq \gamma < |\beta|. \end{aligned} \quad (11)$$

Table 1 shows the restrictions on the dynamical range of the two modes of operation. Since in the calibration mode the spectrum of MIPs will be measured, the resolution must be better than one MIP. For the choice of a low charge bound,  $q_{min} = 0.2$  MIPs, the high bound will be determined by the digitization constant. The digitization constant will also determine the low bound for the physics mode, once the upper bound is set to  $q_{max} = 1540$  MIPs (see Fig. 3). In Table 2 are presented the values of  $q_{max}$  for the calibration mode and of  $q_{min}$  for the physics mode for several choices of the digitization constant.

The dependence of the detector signal on the energy of the particle which initiated the shower is shown in Fig. 4a for several digitization schemes. There is no significant change (energy bias) as a result of the digitization, for the values of  $\mathcal{B}_{digi}$  which were used. The

	Calibration Mode	Physics Mode
$q_{min}$	0.8 fC (0.2 MIPs)	$\sigma_{ADC}$
$q_{max}$	$0.8 \text{ fC} \times 2^{\mathcal{B}_{digi}}$	6 pC (1540 MIPs)

Table 1: Low and high bounds,  $q_{min}$  and  $q_{max}$ , of the dynamical ranges of LumiCal for operation in the calibration (high gain) and in the physics (low gain) modes.

$\mathcal{B}_{digi}$	$q_{max}$ of Calibration Mode	$q_{min}$ of Physics Mode
6	49.9 fC (13 MIPs)	93.7 fC (24 MIPs)
8	199.7 fC (52 MIPs)	23.4 fC (6 MIPs)
10	798.7 fC (205 MIPs)	5.9 fC (1.5 MIPs)
12	3.2 pC (819 MIPs)	1.5 fC (0.4 MIPs)
14	12.8 pC (3277 MIPs)	0.4 fC (0.1 MIPs)

Table 2: Dependence of the high bound,  $q_{max}$ , of the calibration mode, and of the low bound,  $q_{min}$ , of the physics mode on the digitization constant,  $\mathcal{B}_{digi}$ .

important quantity that has to be controlled is the energy resolution, which must be the same for the digitized and the non-digitized cases. [Figure 4b](#) shows the dependence of the energy resolution,  $a_{res}$ , on the digitization constant. [Figure 5](#) shows the dependence of the polar resolution,  $\sigma_\theta$ , and the polar bias,  $\Delta\theta$ , on the digitization constant. The values shown for  $\mathcal{B}_{digi} = 14$  are equivalent to a non-digitized readout (see [Table 2](#)).

For  $\mathcal{B}_{digi} > 8$  it is apparent that the energy resolution, the polar resolution, and the polar bias are all stable. Below this limit there is severe degradation of  $a_{res}$  and slight improvement of  $\sigma_\theta$  and  $\Delta\theta$ . The reason for this is that  $a_{res}$  depends on the accuracy with which each and every detector cell is read-out. This means that fluctuations in  $q_{digi}$  of cells with small energy become critical when  $\sigma_{ADC}$  is large in comparison to the cell signals. On the other hand, the polar angle reconstruction only takes into account contributions from cells with relatively large energy ([Eqs. \(2\) and \(3\)](#)), for which  $\sigma_{ADC}$  is small in comparison. Fluctuations, which hinder the polar reconstruction, decrease for low energy hits.

With the negative influence on the energy resolution being the driving factor, it is concluded that the minimization of  $a_{res}$  requires the digitization constant to be higher than 8.

## 5 Channel Occupancy

The occupancy of LumiCal channels determines the required speed in which the readout electronics must operate. Besides the products of Bhabha scattering, additional particles deposit energy in LumiCal as a result of background processes. The main background to Bhabha scattering is four-fermion processes,  $e^+e^- \rightarrow e^+e^-l^+l^-$ , where  $l = e, \mu, \tau$ . These processes are dominated by two-photon events. Another source of background is beamstrahlung, which is caused by beam-beam interactions.

It has been shown that the dominant process which contributes to the occupancy is beamstrahlung [\[19\]](#). The beamstrahlung electron-positron pair distribution causes continuous low energy depositions at low radii of LumiCal. Since the energy contributions from all incident particles must be read out, the conclusion is that the operating frequency of the electronics must correspond to the bunch repetition rate of the accelerator. For the nominal beam parameters [\[20\]](#), this rate is 3 MHz.

## 6 Summary

The response of the revised design of LumiCal to the passage of minimum ionizing particles and of 250 GeV electron showers has been simulated. These conditions represent the minimal and the maximal cases of energy deposition in LumiCal, respectively. The dynamical range of induced charge in a single LumiCal cell,  $C_{cell}$ , was found to be

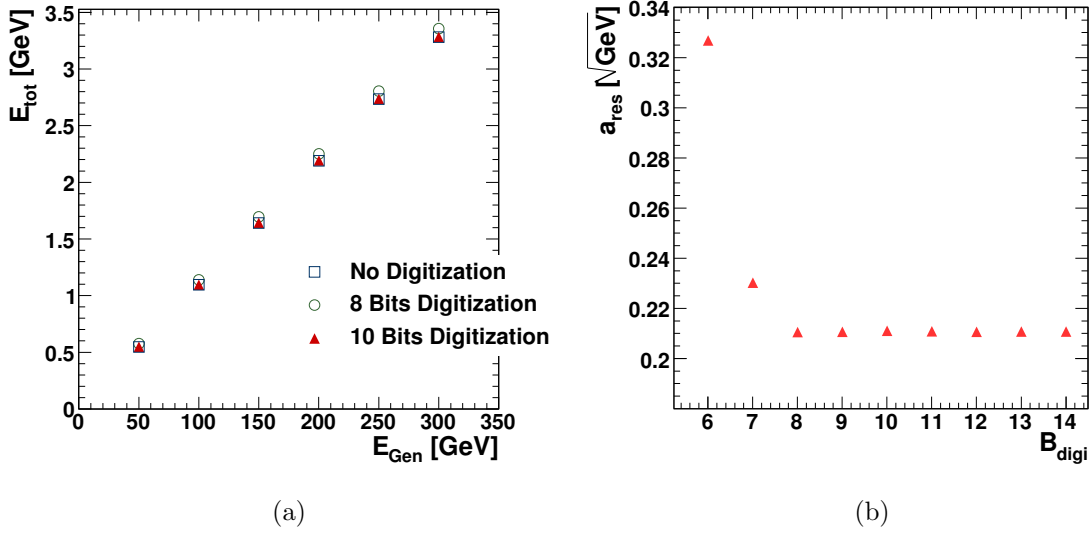


Figure 4: (a) Dependence of the detector signal,  $E_{tot}$ , on the energy of the electron which initiated the shower,  $E_{Gen}$ . The detector signal is either un-digitized, or digitized with 8 or 10 bits, as denoted in the figure. (b) Dependence of the energy resolution,  $a_{res}$ , on the digitization constant,  $B_{digi}$ , for 250 GeV electron showers.

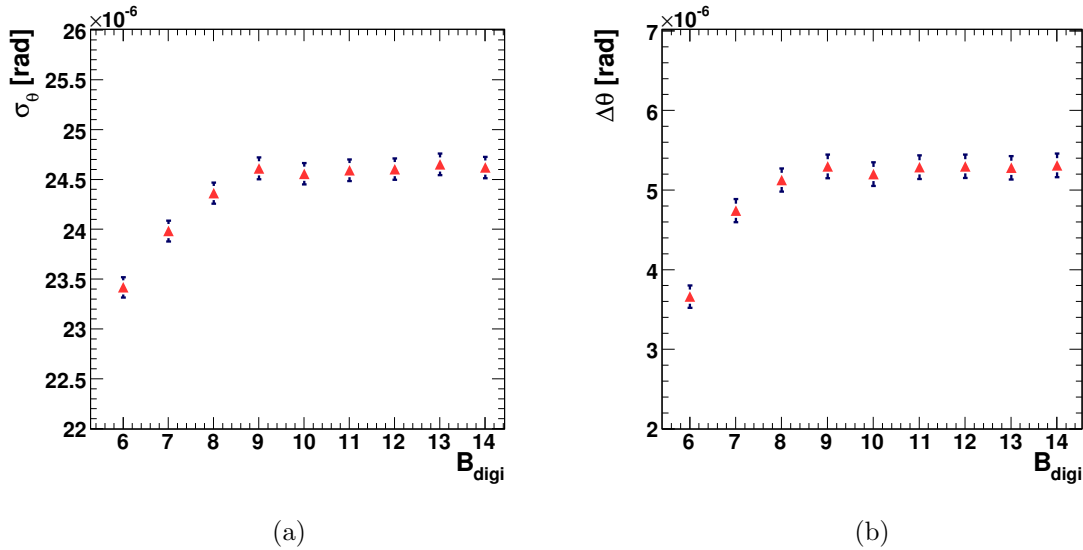


Figure 5: Dependence of the polar resolution,  $\sigma_\theta$ , (a) and of the polar bias,  $\Delta\theta$ , (b) on the digitization constant,  $B_{digi}$ .

$$3.9 < C_{cell} < 6 \cdot 10^3 \text{ fC.}$$

The measurement of MIPs requires a resolution which is better than a single MIP. Several digitization schemes were investigated, and it was shown that in order to simultaneously measure MIPs and high-energy showers, a digitization constant of 14 bits is necessary. Since this choice does not seem feasible, LumiCal will have to be operated in two separate operation modes, a calibration mode for measuring MIP signals, and a physics mode for measuring high energy showers. In this scenario, the digitization constant must be higher than 8 bits, in which case the energy resolution is stable at its minimal value.

The most frequent source of background in LumiCal comes from beamstrahlung electron-positron pairs, which cause continuous inter-bunch energy depositions in LumiCal. The readout electronics must, therefore, be able to discern between the separate deposits from consecutive bunches. This constrains the operation speed of the readout to 3 MHz, in accordance with the nominal ILC running conditions.

## Acknowledgments

This work is partly supported by the Commission of the European Communities under the 6<sup>th</sup> Framework Programme “Structuring the European Research Area”, contract number RII3-026126, and by the Israeli Science Foundation.

## References

- [1] K. Mönig, “Physics Needs for the Forward Region.” Talk given at the Zeuthen FCAL meeting, Aug. 2004.
- [2] T. Becher and K. Melnikov, “Two-loop QED corrections to Bhabha scattering,” *arXiv:0704.3582*.
- [3] S. Actis, M. Czakon, J. Gluza, and T. Riemann, “Two-loop fermionic corrections to massive Bhabha scattering,” *arXiv:0704.2400*.
- [4] A. A. Penin, “Two-loop photonic corrections to massive Bhabha scattering,” *Nucl. Phys. B* *734*, 185, 2006.
- [5] M. Czakon, J. Gluza, and T. Riemann, “The planar four-point master integrals for massive two-loop Bhabha scattering,” *Nucl. Phys. B*, *751*, 1, 2006.
- [6] S. Jadach, “Theoretical error of the luminosity cross section at LEP,” 2003. (hep-ph/0306083).
- [7] “The Large Detector Concept.” URL: <http://www.ilcldc.org/>.

- [8] “The International Large Detector.” URL: <http://www.ilcild.org/>.
- [9] I. Sadeh, “Luminosity Measurement at the International Linear Collider.” URL: [http://alzt.tau.ac.il/~sadeh/mscThesis/iftachSadeh\\_mscThesis.pdf](http://alzt.tau.ac.il/~sadeh/mscThesis/iftachSadeh_mscThesis.pdf), 2008.
- [10] H. Abramowicz *et al.*, “Redefinition of the Geometry of the Luminosity Calorimeter,” *EUDET-Memo-2008-09*, 2008. URL: <http://www.eudet.org>.
- [11] T. C. Awes *et al.*, “A simple method of shower localization and identification in laterally segmented calorimeters,” *Nucl. Inst. Meth. A311*, 130, 1992.
- [12] M. Caffo *et al.*, “Bhabha Scattering,” *Z Physics at LEP1*, *CERN Report 89-08*, 1, 1989. URL: [http://documents.cern.ch/cgi-bin/setlink?base=cernrep&categ=Yellow\\_Report&id=89-08\\_v1](http://documents.cern.ch/cgi-bin/setlink?base=cernrep&categ=Yellow_Report&id=89-08_v1).
- [13] R. Ingbir, “A Luminosity Detector for the International Linear Collider.” URL: <http://alzt.tau.ac.il/~ronen/>, 2006.
- [14] H. Abramowicz *et al.*, “A Luminosity Detector for the International Linear Collider,” *LC-DET-2007-006*, 2007. URL: <http://www-flc.desy.de/lcnotes/notes/LC-DET-2007-006.pdf>.
- [15] I. Sadeh, “Simulation of the performance of LumiCal using MOKKA,” *Talk given at the May 2007 FCAL Collaboration Meeting, DESY-Zeuthen, Germany*. URL: <https://indico.desy.de/conferenceDisplay.py?confId=374>.
- [16] M. Battaglia *et al.*, “Contrasting Supersymmetry and Universal Extra Dimensions at colliders,” *arXiv:hep-ph/0507284*.
- [17] “MOKKA - a detailed GEANT4 detector simulation for the Future Linear Collider.” URL: <http://polywww.in2p3.fr/geant4/tesla/www/mokka/mokka.html>.
- [18] J. Allison *et al.*, “GEANT4 developments and applications,” *IEEE Transactions on Nuclear Science*, 53, No. 1, 270-278, 2006.
- [19] B. Pawlik, “Estimation of physics and beamstrahlung background in Luminosity measurements,” *Talk given at the May 2008 FCAL Collaboration Meeting, IFJ PAN, Krakow, Poland*. URL: <http://www.ifj.edu.pl/conf/fcal/fcal2008/>.
- [20] Nan Phinney *et al.*, “ILC Reference Design Report Volume 3 - Accelerator,” *arXiv:0712.2361v1*.